Scaling of deuterium retention in < 3 MeV proton damaged Beryllium, Eurofer, and W-5Re in the range of 0.0003 to 6 DPA

S. Möller*, A. Kreter, N. Helfer, N. Aghdassi, R. Rayaprolu, M. Rasinski, T. Dittmar, M. Flebbe, and Ch. Linsmeier
Forschungszentrum Jülich GmbH, Institut für Energie- und Klimaforschung, 52425 Jülich,

E-mail: s.moeller@fz-juelich.de

Received xxxxxx
Accepted for publication xxxxxx
Published xxxxxx

Abstract

In continuation of earlier work on 3 MeV proton-damaged tungsten and reduced-activation steels we present new results on Eurofer97, Beryllium and W-5%Re sintered alloy irradiated <400 K. Methodical improvements result in largely reduced uncertainties. Beryllium is loaded using a 5 kV D_2^+ ion-source to $6.3*10^{21}$ D/m² at 300 K. Eurofer97 and W-5Re are loaded in PSI-2 to $3*10^{25}$ D/m². Irradiation and D-loading are conducted at ~400 K. The D retention is measured by ^{3}He µ-NRA. An exponential saturation fits the W-5Re D-retention data with R^2=0.99 . The retention increases by a factor 10.3 in W-5Re, similar as in W, but on 10 times lower level. Retention in Eurofer97 proves to be independent of displacement damage up to 6.3 DPA (±25%). Beryllium shows increased retention by a factor 3 up to the maximum of 0.08 DPA. The retention in beryllium starts saturating, but the limited DPA range allows fitting the data with exponentials and power-laws.

Keywords: nuclear fusion, radiation damage, accelerator technology, hydrogen retention, plasma-facing materials, ion beam analysis

1. Introduction

Hydrogen isotope retention in fusion relevant materials potentially induces risks for nuclear safety and tritium self-sufficiency of future fusion power reactors. The safety aspect is in particular relevant for ITER, since retention potentially limits ITER operation due to legal limits on the radioactive inventory [1]. Power reactors such as DEMO will further push the material damage with rates of ~5 displacements per atom (DPA) per year and ~500 ppm Re/year in W [2], resulting, with expected 10 year lifetimes, in 50 DPA and 5% Re.

For testing these altered materials, the materials can be damaged by neutrons and ions [3]. 3 MeV protons offer the advantages of non-active handling and high DPA rates, at the expense of only affecting the first few 10 µm and grains at the material surface [4]. While 3 MeV protons induce fewer displacements per ion (DPI) compared to heavy ion irradiation, this physical disadvantage is compensated by technical aspects resulting in largely higher beam currents and smaller beam spots achievable with protons. TEM observations with similar proton irradiated materials showed increasing defect density with DPA up to a saturation limit around 0.2 DPA in tungsten from where on mostly the loop defect size increased with constant loop density [5]. Also [6] found saturation effects in the 0.2 DPA region with a factor 5.5 increase in retention at 300 K, but by using heavy ions with 1 µm damage range. Protons with ~15 µm range showed a significantly higher factor of ~13 increase for D retention in W [4]. In spite of the different increase factors, saturation concentrations in the order of 1-2 at.% were seen regardless of the irradiation method. D-retention is typically seen to be largest in the first µm of the exposed surface, a situation probably reducing the increase factor of D-retention differently for the comparable range of heavy ions compared to the >10 times larger range of protons, but also the concept

of a universal behaviour of different material grades at high DPA levels remains an open question.. A clustering of normally solute Re in W to Re enriched phases was observed under irradiation [7], potentially imposing a difference between D-retention in pristine W-Re alloys, the displacement damage, and the transmuted W-Re compound.

For steels the situation is more difficult. The retention is in any case lower compared to W, often at the detection limits of the typical methods such as nuclear reaction analysis (NRA) and near the natural D background due to the presence of H. After 20 MeV W-ion irradiation of Eurofer97 (Eu97) up to 1.13 DPA near room temperature, a slight increase up to a few 0.1 at.% D was observed in [8], but it remains unclear whether this relates to the implanted W ions or the lattice damage. The study of CLF-1, a RAFM steel similar to Eu97, revealed slight increases in the order of a few 10% up to about 4 DPA of Fe ion damage at ~340 K [9]. In [10] similarly no significant increase in retention was found for different steels at 460 K and higher, although at room temperature increases of a factor 10 were observed. Higher retention and a remarkable increase with DPA was reported in our former study for the purely ferritic and precipitate hardened HiperFer [4] at 400 K. These results indicate the importance of phase structure and composition for damage accumulation and retention in steels. Furthermore, it seems that a critical temperature in the range of 400-600 K exists, at least for Eurofer and structurally similar steels, above which the retention becomes independent of displacement damage.

Studies of neutron irradiated Be mostly focus on tritium production in pebbles [11] or mechanical properties[12]. The retention after 40 DPA fission neutron irradiation and T_2-gas loading increased by a factor 10 over the unirradiated case to about 0.1 at% [13] and by a factor 15-43 and up to 0.125 at.% [14] at 1.6 DPA with T loading temperatures up to 1100 K in both cases. Very recently the first study on oxygen ion irradiated and subsequently plasma exposed beryllium was published [15], showing an 18% decrease in D-retention in beryllium at 370 K and 573 K plasma exposures damaged to ≥0.1 DPA, an open research question arises from this counterintuitive result [16].

This work continues the investigation of the deuterium retention with irradiated polished W-5Re, Eu-97, and Be after different levels of displacement damage induced by 1.45 to 2.96 MeV protons at ~400 K. Methodical improvements will be presented resulting in largely reduced uncertainties. The data interpretation focusses on scalings and increase factors to mitigate the impact of material properties (impurities, defect density…) and storage time (outgassing, isotope exchange, annealing…), which largely vary between studies, on the outcome.

2. Experimental setup

Polished ($R_a \leq 20$ nm) 10x10x5 mm³ samples with a 1 mm step for clamping are made from hot-pressed high purity powders of W and Re (compositional data in the appendix) and Eu-97 steel sheet metal. The Beryllium sample is made from polycrystalline 99.5% purity (mostly Fe and O) material in a shape of 10x10x0.45 mm³. The W-5Re material features grain sizes in the order of ~100 µm and a scarce porosity with ~1 µm diameter pores. Only thin (<100 nm) damage layers due to polishing were observed by FIB/SEM analysis in similar samples before. No pre-outgassing of residual hydrogen is conducted. The sample irradiation is done in a 1.7 MV tandem DC accelerator in combination with a triple-quadrupole focus magnet and a chamber usually used for ion beam analysis (IBA). The chamber provides a pressure of $8\pm2*10^{-8}$ mbar during irradiation.

The radiation protection aspects of this irradiation method were discussed in [4]. Two new elements have to be considered in this study, rhenium and beryllium. Beryllium itself can only produce long-term activation via ^{9}Be(p, t)^{7}Be with a threshold at 13.4 MeV. The zero threshold reaction produce only stable products and fast ions. The reaction ^{9}Be(p, n) results in ^{9}B, which decays into a proton and two α particles, but it generates massive neutron radiation dose rates above its threshold of 2.05 MeV. The ^{9}Be(p, pn) reactions have even slightly lower thresholds down to 1.75 MeV. For mechanical reasons beryllium metal typically contains a few 100 ppm of iron, resulting in the production of Co isotopes, and uranium as main mining related impurity. For iron, the same considerations as for steels apply. Due to this and the low concentration, no relevant activity is observed. For Re, the reaction ^{185}Re(p, n)^{185}Os produces the ^{185}Os isotope with 93.8 days half-life and relevant γ-emission. Calculations predict an activity of 0.2 mBq at the given irradiation doses and Re concentration, way below any detection or release limits and the activity produced from the tungsten part of the sample. In conclusion, the methodology can be applied to W-Re alloys without any changes and to Be with energies <2 MeV. Interestingly, avoiding nuclear problems results in similar proton ranges in the order of 30 µm for all 3 metals, in spite of their largely different nuclear masses.

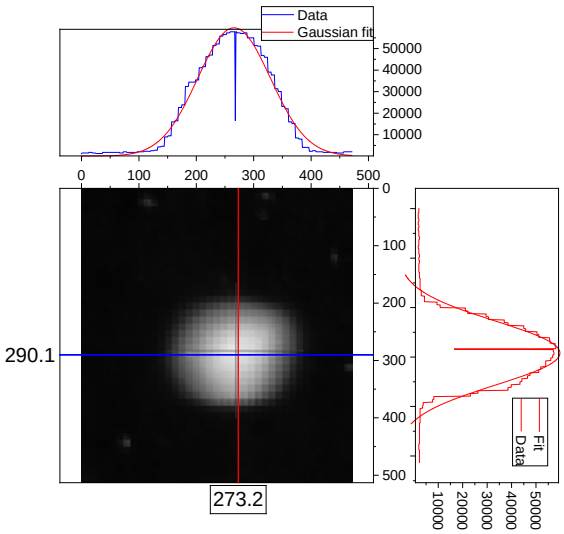

Figure 1: Exemplary camera image of the irradiation spot scintillation light intensity with coordinates in pixel (1 Pixel =2.1 µm). The spot features a Gaussian peak profile with a FWHM width of 109±3 pixel. Units are pixels and digital levels.

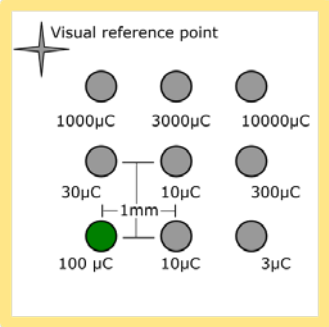

Figure 2: The matrix spot irradiation scheme aligned by a visual reference at the sample edge. The irradiation starts at the lower left point (green) with low doses allowing the sample to heat up before reaching higher doses. The figure shows the total doses of each spot. For practical reasons a 2 mm spacing was applied together with larger spots for the beryllium sample.

Figure 1 illustrates the typical spot-size measurement using a $LiAlO_2$ single crystal with a reduced beam current of ~30 nA (reduction of the stripper gas density). We find a 400 µm (W-5Re, Eu97) and 900 µm (Be) total diameter spot, respectively, with a Gaussian current distribution. Taking the FWHM size of the spots results in 230±7 µm and 518±15µm, respectively. The 76% of the total current hits the FWHM spot. The sample temperature is measured via a type-K thermocouple attached to the sample back during irradiation to 333 K (W-5Re and Eu97) and 300 K (Be), respectively. The temperature stabilises after about 1 minute as would be expected from the sample heat capacities and the beam power. Consequently, a non-constant temperature can be expected only for the first irradiation spot, see Figure 2. The heat flux of the focussed ion beam increases the surface temperature in the spot by additional 30 K (W-5Re, Be) and 104 K (Eu97 irradiation temperature = 437±10 K), respectively, as finite element simulations predict. Since the sub-mm beam spot sits in a 10 mm sized sample without any contacts or coolants we consider the simulations accurate.

Inspired by the earlier study, this study implements more low DPA points and a systematic software controlled irradiation spot matrix pattern for reduced relative uncertainties in the post-analysis and more information in the region <0.2 DPA. W-5Re and Eurofer are irradiated on 9 spots in a quadratic 1 mm spacing grid as shown in Figure 2. The same grid applies to Be but with 2 mm spacing. The highest irradiation doses of 10 mC could not be achieved due to limits of the working shifts. Instead, the Eu-97 sample received a dose of 9.727 mC, W-5Re of 9.366 mC and Be of 1.33 mC in the upper-right spot, see Figure 2.

For DPA calculation in beryllium the SRIM 2013 code in the *Quick Calculation of Damage* mode is used according to agreed standards [17], [18] in a similar fashion as described in [4]. Beryllium features only a scarce data situation, but [19] states a displacement threshold of 21 eV resulting in 14.6 displacements per ion (DPI) within a range of 29.2 µm for 1.45 MeV protons. The homogeneous range corresponding to an increase of the DPI per length of 20% above the surface value is 17 µm with 2.4 DPI. Due to the different DPI every material receives different DPA levels within the relevant depth with the given ion doses. The low DPI values and the requirements of larger spots for post analysis strongly limited the DPA in beryllium. The damage rates are ~10^{-4} DPA/s in W-5Re and Eu97 and 10^{-5} DPA/s in Be.

The effects of H implantation were discussed in the former study [4] at the example of W and steel. It was shown, that the amount of protons deposited within the homogeneous damage range remains negligible with implanted fractions between 10^{-5} and 10^{-4}. New SRIM calculations confirm ~10^{-5} for Be and ~10^{-4} for W-5Re. The D retention shown later exceeds the implanted H concentration by two orders of magnitude for Be and W-5Re. For Eu97 the values of H and D are comparable. At the terminal proton range an optically visible subsurface blister can form due to the massive implantation. The blister evolution can be suppressed by irradiating the sample above a material-dependent temperature, which is achieved in this work for all investigated materials. Consequently, we consider the influence of H implantation negligible.

After irradiation, the Eu97 and W-5Re samples are loaded by D_2 plasma in PSI-2[20] with identical settings as in [4]. The samples are exposed on the axial manipulator using a Mo mask. The sample temperatures are kept at 400±30 K. The plasma provides a peak flux density of 1.6±0.5*10^{21} D/m²s at an electron temperature of ~8 eV for 5.25 h resulting in a fluence of 3±0.8*10^{25} D/m². A bias of 65 V is applied to the sample holder resulting in ~45 eV ion impact energy. The Beryllium sample is loaded by a SPECS IQE 12/38 ion source with 5 kV acceleration potential and 45° impact angle with

respect to the surface normal. The implantation spot has a mostly circular form of 6.5mm radius. The source delivers a current of 1 µA for 24 h onto this spot resulting in a total fluence of $6.3*10^{21}$ D/m² and a beam heat load of 5 mW. The sample remains at about 300 K during ion implantation with only ~1 K increase due to the beam loading. This source type provides >93% of D_2^+ ions, resulting in 2.5 keV impact energy per D ion. The remainder of 7% is mostly D^+ ions. For 2.5 keV D SRIM calculations show an average implantation depth of 44 nm with a broad distribution of 20 nm FWHM. The sputter yield remains at 0 for 10^5 histories, but in the range down to 70 nm 6.2 displacements are induced on average per ion, dominating over the damage induced by the high energy protons in this depth range. The chamber features a background pressure of $5*10^{-9}$ mbar during implantation.

After D exposure, the retention is analysed via 2.96 MeV $^3He^+$ ion-beam analysis in the µNRA device [21]. The beam is focused to a spot size of 120-150 µm (W-5Re) and 200 µm (Be), respectively, about half the irradiation spot FWHM diameter. The irradiation spots are invisible in the positioning camera, hence reference markings and the spot matrix irradiation pattern are used for positioning. In a 50 µm window, the exact position of highest measured D retention is selected for aligning the matrix. The spot matrix scheme reduces the relative alignment uncertainties to negligible 20 nm, but a systematic misalignment of all spots (a matrix offset) in the order of 50 µm remains possible. Together with irradiation spot size we end up with a 15% systematic uncertainty in the given DPA levels, depending where the analysis spot sits inside the FWHM zone (centre vs. edge). Consequently, we do not expect an impact on the trend of analysis of Retention vs. DPA, since this relative uncertainty is negligible. The spectra are analysed via SimNRA 7.03 [1] with D(^{3}He, p)^{4}He cross-section from [22]. The Particle*Sr value is determined using the RBS part and constant ion dose of 4 µC is applied on all analysed spots. The measurement of the Eu97 and the W-5Re samples is executed about 9 month after exposure with storage mostly in vacuum and 4 days after exposure for the beryllium sample. Statistical measurement uncertainties due to counting, geometry, and Particle*Sr sum up to 5-15% with D(^{3}He, p)^{4}He counts between 100 and 1000 for Be and W-5Re. In the case of Eu97 low counting statistics of ~20 counts increase this uncertainty to 25%.

3. Results

The exposures resulted in no visible surface modifications. Electron microscopy (SEM) and focussed ion-beam cross-sectioning (FIB) revealed the formation of <20 nm thick blister volumes at ~130 nm depth and with ~100 nm diameter in the W-5Re sample, see Figure 3. These blisters occur preferentially on certain grains, independent of the irradiation. No surface modifications are observed on the Eu97 sample. The Be sample could not be analysed by SEM for safety reasons. Interestingly the proton irradiation spots are not visible in the SEM pictures, but only the ^{3}He NRA analysis spots can be seen as darker regions, see Figure 4. From this the spot size is determined to ~137 µm rectangles on the W-5Re sample, confirming the analysis spot size claimed above. The electron backscatter diffraction (EBSD) mapping of the highest DPA spot on the W-5Re sample revealed no clear changes in grain structure due to the irradiation, see Figure 5.

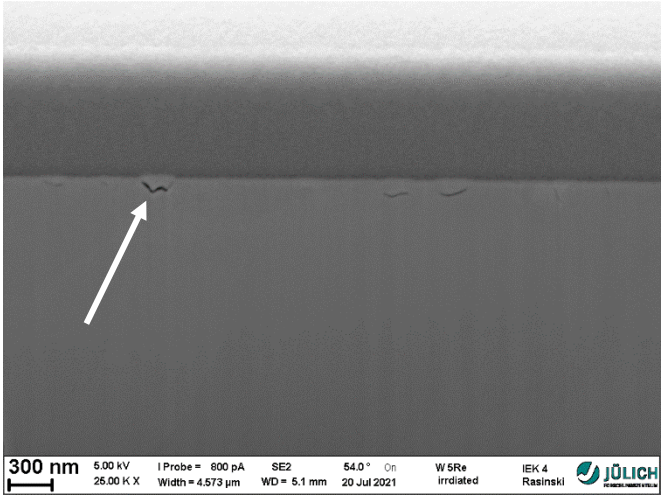

Figure 3: SEM image of a FIB cut showing the blister volumes in the W-5Re sample (arrow)

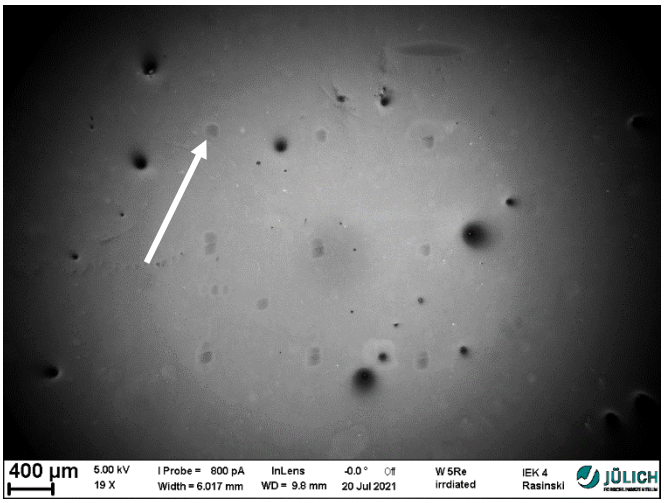

Figure 4: SEM image showing the NRA analysis spots as darker regions. The arrow indicates one of the spots.

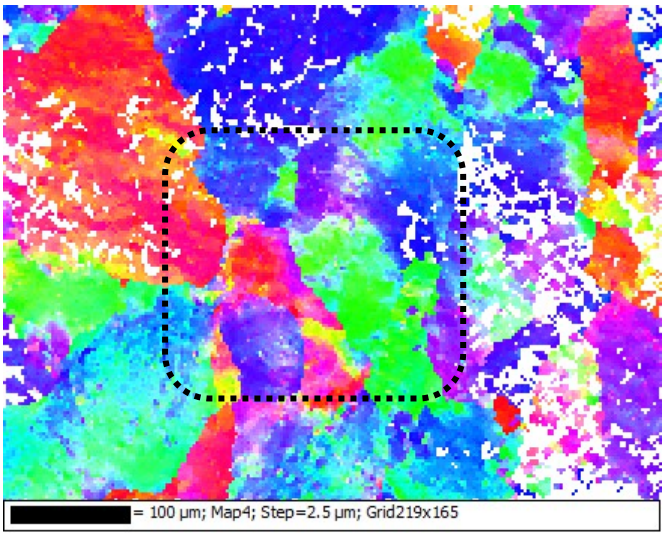

Figure 5: EBSD map of the highest DPA spot on the W-5Re sample. The dotted box shows the proton irradiation spot, but no clear structural change can be observed. The EBSD evaluation failed in the white spots.

Figure 6 shows the retention and damage values investigated in the irradiated and the unirradiated reference cases (0 DPA). NRA shows minor surface contamination by C and O. D depth profiles measured in all samples with a depth resolution of 2 µm show the retention limits to <=2 µm depth. This is in contrast to the former study on pure W, where D was also found down to 4 µm [4]. Better-resolved depth profiles could not be obtained. Consequently, the NRA analysis catches all of the D in the samples.

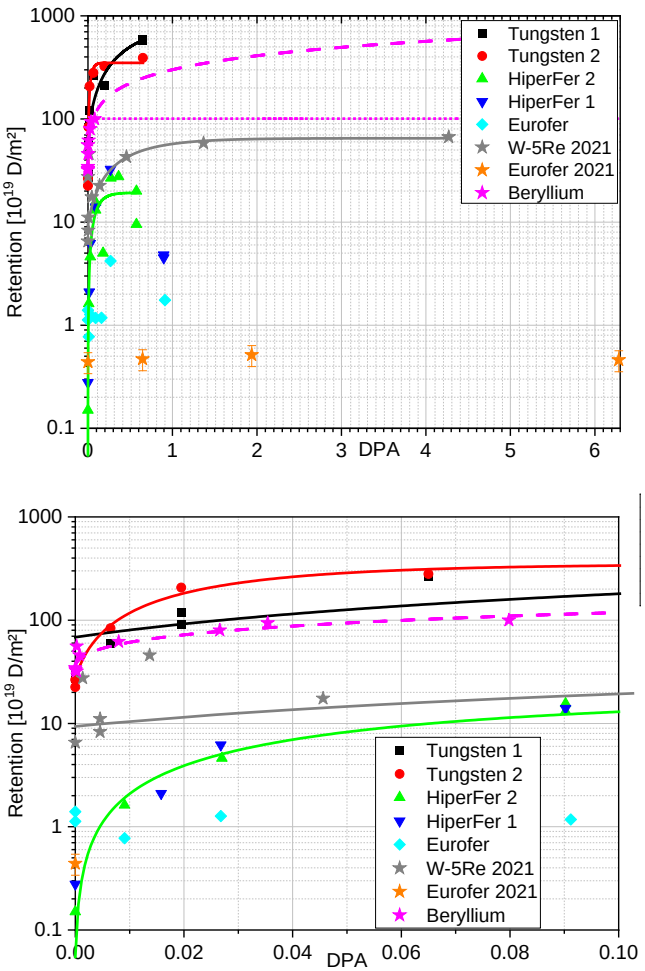

Figure 6: Plot of the relation between NRA retention (~2 µm) and DPA together with fits in two different magnifications. The new data (stars) are plotted together with data from [4]. For beryllium, the exponential fit (dotted) is compared to a square-root fit (dashed), showing large deviations in the extrapolation region in spite of similar R^2=0.9. Relative uncertainties are within the marker sizes except for the new data "Eurofer 2021". The absolute uncertainty is larger with 15% in both axes.

At low DPA, the D retention increases strongly with damage in both W-5Re and beryllium. This increase saturates in W5-Re at ~0.2 DPA. The lines drawn in Figure 6 represent this with a good agreement to an exponential decay function with offset with the resulting fit of W-5Re shown in equation 1. An exponential saturation fits the W-5Re D-retention data with a coefficient of determination of R^2=0.99, when neglecting the two outliers <0.01 DPA. The saturation retention level lies in W a factor 10.3 above the un-irradiated W-5Re compared to a value of 13-20 for pure W found in [4]. For beryllium a factor 3±0.3 increase is found for the highest level of 0.08 DPA. Considering the limited range of D diffusion into the materials at the given exposure temperatures, a saturation of the available traps is expected for all samples within the first 2 µm.

$$Retention\left[\frac{10^{19}D}{m^2}\right] = 65 \pm 2.3 - 55.6 \pm 2.5 * e^{-\frac{DPA}{0.51 \pm 0.01}} \quad (1)$$

4. Conclusions

Technical improvements of focused proton beam irradiation allowed increasing the amount of maximum DPA by an order of magnitude, the amount of DPA steps by a factor 2 and the relative accuracy by a factor 5 with respect to the earlier study. The investigation of irradiated samples benefits from focused proton irradiation by identical plasma exposure and bulk material properties, high throughput and identical storage and surface conditions for all irradiation levels. As drawbacks different irradiation temperatures can occur depending on the beam current stability (~1% for modern accelerators) and the irradiation spots potentially hit only a single grain, inducing systematic differences in the material properties between different DPA levels, if grain and spot size are of similar order. In general, we expect this method to minimize the level of systematic uncertainties against non-focussed irradiation approaches. This resulted in an exceptional reproducibility of the retention results, in particular for an irradiation damage study. This enabled extending the former dataset on retention after 3 MeV proton irradiation to two additional fusion relevant materials and results in more robust inter- and extrapolations.

In W-5Re we see a clear trend similar to pure W with a saturation onset at ~0.2 DPA and a factor 10.3 increase in retention. The overall level of retention in W in the former study exceeded the new values of W-5Re by a factor ~5. While the lower retention in W-5Re compared to W qualitatively agrees to literature findings, the reduction factor found here is significantly higher. The 0.06 wt.% impurity content in the used W-5Re appears to be negligible for the D retention, since its value is 20x higher than the measured impurities in the W used in the former study and more impurities should not decrease the D retention (see analysis results in the appendix). The W was rolled during manufacturing while the W-5Re was only hot pressed with some remaining porosity and the materials also show different grain sizes. This indicates defects dominate the long-term retention in both W and W-5Re and potentially also influence the annealing and defect agglomeration dynamics responsible for D trapping alongside the Re content. Consequently, the data suggest a negligible direct impact of the transmutation elements in W in a DEMO reactor, but we have to understand the dynamics of point defects for realistic predictions of retention under combined irradiation damage. The shallower penetration depth of D in W-5Re indicated a possible further contribution to lower retention in W-5Re in this study through limited D penetration and increased outgassing during loading compared to the former study. The observed formation of subsurface nano-bubbles may have an impact on total retention, but as the SEM analyses shows, the bubbles occur independent of the irradiation. Furthermore, even at the highest DPA levels no change of grain structure or amorphisation is visible through EBSD analysis. In conclusion, the results suggest only little influence of porosity, impurities, and Re content on the hydrogen retention in W. No further increase of retention in W is expected from our data for higher displacement damage levels and the correlated built-up of Re and other transmutation elements and porosity in a fusion power reactor.

For Eu97, the former data were confirmed showing no statistically significant increase in retention due to irradiation, within the 25% uncertainty margin, in agreement with literature of RAFM steels. The retention levels are anyways low in Eu97, but the increased DPA levels and NRA detection limits, compared to our former study, made no difference. The outgassing during the 9 month storage between exposure and analysis and the different material batches could be factors for the generally ~2x lower retention observed here compared to the former study. Possibly the induced traps already outgas or even anneal at 400 K or within the 9 month storage at room temperature in Eu97, limiting the total retention but also its increase with DPA. This finding agrees with literature, narrowing down the temperature where the radiation induced defects anneal in a way that the D-retention remains independent of DPA to the range of ~360-437 K.

Anyways, from a practical point of view our results recommend Eu97 in comparison to all other tested materials for situations where high radiation damage levels are expected and hydrogen retention is critical, since a complete outgassing within ≤9 month or above 400 K will anyways strongly limit the retention in a fusion reactor.

For the first time the method of MeV proton irradiation damage testing was successfully applied to Beryllium. The beam on-radiation represents a technical problem, but we showed similar damage ranges as for the other materials can be obtained with practically zero beam-on radiation or activation when using 1.45 MeV protons. A factor 3 increase and saturating behaviour was found here already <0.1 DPA. Interestingly, we see already 25% of the increase seen at 1.6 DPA in the literature within <0.1 DPA. The square-root fit of our data (Figure 3) matches our data to the increase factor for the higher DPA levels investigated in the literature. Our findings oppose the findings of the only similar study [15]. Anyways, the methodological differences hardly allow for any credible comparisons and data are scarce, demanding further detailed experimental investigation, which are now possible with our newly established methodology for beryllium. For plasma facing materials this increase in retention and our observed limited depth penetration suggest still a negligible contribution compared to the expected retention in co-deposited Be layers. For other Be components, e.g. for T

breeding, our data predict a significant increase of the retention with irradiation.

Our spot matrix method enables further increased point density of several 100 points to be fitted onto a single sample. A new setup with improved beam power handling capabilities is currently being installed for increasing the beam current and adding active temperature control up to 1200 K. With these additions we aim at inducing a fine grid of data-points over 5 orders of magnitude of DPA up to fusion relevant material service-lifetimes of about 50 DPA in tungsten in future studies. Furthermore, TEM analysis and post-mortem annealing of the samples together with re-loading in PSI-2 will enable addressing the fundamental dynamics of defects in the investigated materials.

Acknowledgements

The authors thank the PSI-2 Team, especially Michael Vogel and Sebastian Kraus for the reliable device operation.

This work has been carried out within the framework of the EUROfusion Consortium and has received funding from the Euratom research and training programme 2014-2018 and 2019-2020 under grant agreement No 633053. The views and opinions expressed herein do not necessarily reflect those of the European Commission.

Appendix

Certificate of Analysis

Materials				Tungsten Rhenium 95/5wt%							
Purity				W + Re ≥99.95%							
Elements	Actual	Spec	Units	Elements	Actual	Spec	Units	Elements	Actual	Spec	Units
Li			ppm	Zn			ppm	Pb	15		ppm
B			ppm	Ga			ppm	Bi	10		ppm
F			ppm	Ge			ppm	Y			ppm
Na			ppm	As	15		ppm	Th			ppm
Mg	60		ppm	Se	25		ppm	Er			ppm
Al	8		ppm	Zr			ppm	Re	4.92		wt%
Si	15		ppm	Nb			ppm	Ru			ppm
P	50		ppm	Mo	25		ppm	Rh			ppm
Cl			ppm	Pd			ppm	Os			ppm
K			ppm	Ag			ppm	Cs			ppm
Ca	15		ppm	Sn	10		ppm	Cd			ppm
Ti			ppm	Sb	15		ppm				ppm
V			ppm	Ba			ppm				
Cr			ppm	Hf			ppm				
Mn			ppm	Ta			ppm	C	25		ppm
Fe	25		ppm	W	Matrix		wt%	S			ppm
Co			ppm	Pt			ppm	O			ppm
Ni	40		ppm	Au			ppm	N	25		ppm
Cu	30		ppm	Hg			ppm	H			ppm

Figure 7: Manufacturer ICP-OES purity analysis of the used W-5Re. The data reveal an impurity content of about 400 weight ppm.

Element	Manufacturer's Specifications [µg/g]	As determined by ICP [µg/g]
Al	15	< 3
Fe	30	7.1
Si	20	
H	5	0.0001
Cd	5	0.01
Cr	20	3.18
K	10	< 30
Mo	100	6
N	5	0.0004
Hg	1	< 2
Cu	10	< 0.7
Ni	20	< 10
C	30	0,0012
O	20	0,0004
Pb	5	< 0.008
Re	0	< 0.5
Ta	0	< 2
S	0	<0.0013

Figure 8: Purity analysis of the Plansee W used in [4]. The analysis revealed a purity exceeding the specification by one order of magnitude with about 20 weight ppm of impurities compared to the specified 99.97% purity.

References

[1] J. Roth *et al.*, 'Tritium inventory in ITER plasma-facing materials and tritium removal procedures', *Plasma Phys. Control. Fusion*, vol. 50, no. 10, p. 103001, Aug. 2008, doi: 10.1088/0741-3335/50/10/103001.

[2] Mark R. Gilbert Jean-Christophe Sublet, 'Handbook of activation, transmutation, and radiation damage properties of the elements simulated using FISPACT-II & TENDL-2015; Magnetic Fusion Plants'. CCFE, 2016.

[3] R. Rayaprolu, S. Möller, Ch. Linsmeier, and S. Spellerberg, 'Simulation of neutron irradiation damage in tungsten using higher energy protons', *Nuclear Materials and Energy*, vol. 9, pp. 29–35, Dec. 2016, doi: 10.1016/j.nme.2016.09.008.

[4] S. Möller, R. Krug, R. Rayaprolu, B. Kuhn, E. Joußen, and A. Kreter, 'Deuterium retention in tungsten and reduced activation steels after 3 MeV proton irradiation', *Nuclear Materials and Energy*, p. 100742, Mar. 2020, doi: 10.1016/j.nme.2020.100742.

[5] R. Rayaprolu, S. Möller, R. Abernethy, M. Rasinski, J. C. Haley, and Ch. Linsmeier, 'Indentation testing on 3 MeV proton irradiated tungsten', *Nuclear Materials and Energy*, vol. 25, p. 100776, Dec. 2020, doi: 10.1016/j.nme.2020.100776.

[6] G. R. Tynan *et al.*, 'Deuterium retention and thermal conductivity in ion-beam displacement-damaged tungsten', *Nuclear Materials and Energy*, vol. 12, pp. 164–168, Aug. 2017, doi: 10.1016/j.nme.2017.03.024.

[7] A. Xu *et al.*, 'Ion-irradiation-induced clustering in W–Re and W–Re–Os alloys: A comparative study using atom probe tomography and nanoindentation measurements', *Acta Materialia*, vol. 87, pp. 121–127, Apr. 2015, doi: 10.1016/j.actamat.2014.12.049.

[8] O. V. Ogorodnikova and K. Sugiyama, 'Effect of radiation-induced damage on deuterium retention in tungsten, tungsten coatings and Eurofer', *Journal of Nuclear Materials*, vol. 442, no. 1, pp. 518–527, Nov. 2013, doi: 10.1016/j.jnucmat.2013.07.024.

[9] L. Qiao, X. Zhang, R. He, H. Zhang, and P. Wang, 'Influences of displacement damage due to heavy ion

irradiation on deuterium retention in CLF-1 steel', *Nuclear Materials and Energy*, vol. 25, p. 100794, Dec. 2020, doi: 10.1016/j.nme.2020.100794.

[10] O. V. Ogorodnikova *et al.*, 'Surface modification and deuterium retention in reduced-activation steels under low-energy deuterium plasma exposure. Part II: steels pre-damaged with 20 MeV W ions and high heat flux', *Nuclear Fusion*, vol. 57, no. 3, p. 036011, Mar. 2017, doi: 10.1088/1741-4326/57/3/036011.

[11] V. Chakin *et al.*, 'Tritium release and retention properties of highly neutron-irradiated beryllium pebbles from HIDOBE-01 experiment', *Journal of Nuclear Materials*, vol. 442, no. 1, Supplement 1, pp. S483–S489, Nov. 2013, doi: 10.1016/j.jnucmat.2013.03.032.

[12] V. Barabash, G. Federici, M. Rödig, L. L. Snead, and C. H. Wu, 'Neutron irradiation effects on plasma facing materials', *Journal of Nuclear Materials*, vol. 283–287, pp. 138–146, Dec. 2000, doi: 10.1016/S0022-3115(00)00203-8.

[13] H. Kwast, H. Werle, and C. H. Wu, 'Tritium retention in neutron-irradiated carbon-based materials and beryllium', *Phys. Scr.*, vol. T64, pp. 41–47, Jan. 1996, doi: 10.1088/0031-8949/1996/T64/006.

[14] C. H. Wu *et al.*, 'EU results on neutron effects on PFC materials', *Fusion Engineering and Design*, vol. 39–40, pp. 263–273, Sep. 1998, doi: 10.1016/S0920-3796(98)00196-3.

[15] A. Založnik, R. P. Doerner, T. Schwarz-Selinger, M. Miyamoto, and S. Brezinsek, 'Deuterium retention in MeV ion-irradiated beryllium', *Journal of Nuclear Materials*, p. 153139, Jun. 2021, doi: 10.1016/j.jnucmat.2021.153139.

[16] G. De Temmerman *et al.*, 'Data on erosion and hydrogen fuel retention in Beryllium plasma-facing materials', *Nuclear Materials and Energy*, vol. 27, p. 100994, Jun. 2021, doi: 10.1016/j.nme.2021.100994.

[17] 'ASTM Standard E521-96. Standard practice for neutron radiation damage simulation by charged-particle irradiation'. 2009.

[18] R. E. Stoller, M. B. Toloczko, G. S. Was, A. G. Certain, S. Dwaraknath, and F. A. Garner, 'On the use of SRIM for computing radiation damage exposure', *Nuclear Instruments and Methods in Physics Research Section B: Beam Interactions with Materials and Atoms*, vol. 310, pp. 75–80, Sep. 2013, doi: 10.1016/j.nimb.2013.05.008.

[19] V. A. Borodin and P. V. Vladimirov, 'Damage production in atomic displacement cascades in beryllium', *Nuclear Materials and Energy*, vol. 9, pp. 216–220, Dec. 2016, doi: 10.1016/j.nme.2016.07.001.

[20] A. Kreter *et al.*, 'Linear Plasma Device PSI-2 for Plasma-Material Interaction Studies', *Fusion Science and Technology*, vol. 68, no. 1, pp. 8–14, Jul. 2015, doi: 10.13182/FST14-906.

[21] S. Möller *et al.*, 'A New High-Throughput Focused MeV Ion-Beam Analysis Setup', *Instruments*, vol. 5, no. 1, Art. no. 1, Mar. 2021, doi: 10.3390/instruments5010010.

[22] V. Kh. Alimov, M. Mayer, and J. Roth, 'Differential cross-section of the D(3He,p)4He nuclear reaction and depth profiling of deuterium up to large depths', *Nuclear Instruments and Methods in Physics Research Section B: Beam Interactions with Materials and Atoms*, vol. 234, no. 3, pp. 169–175, Jun. 2005, doi: 10.1016/j.nimb.2005.01.009.